



The effect of overshooting 1.5°C global warming on the mass loss of the Greenland Ice Sheet

Martin Rückamp¹, Ulrike Falk¹, Katja Frieler², Stefan Lange², and Angelika Humbert^{1,3}

¹Alfred Wegener Institute, Helmholtz Centre for Polar and Marine Research, Bremerhaven, Germany

²Potsdam Institute for Climate Impact Research, Potsdam, Germany

³University of Bremen, Bremen, Germany

Correspondence to: martin.rueckamp@awi.de

Abstract. Sea level rise associated with changing climate is expected to pose a major challenge for societies. Here, we estimate the future contribution of the Greenland ice sheet (GrIS) to sea level change in terms of different ice sheet atmospheric forcings arising from three general circulation models (GCMs), HadGEM2-ES, IPSL-CM5A-LR and MIROC5, for RCP2.6. We run the ice sheet model ISSM with higher order approximation and use a spin-up/inversion scheme to estimate the present day state.

5 The forcing fields for surface mass balance (SMB) and ice surface temperature (T_s) are computed by the SEMIC model (Krapp et al., 2017) and applied as anomalies to RACMO2.3 fields. According to the three GCMs, warming of 1.5°C has been reached at GrIS by 2005 (HadGEM2-ES, MIROC5) or as early as 1995 (IPSL-CM5A-LR). Forcing fields suffer from underestimation of polar amplification (MIROC5) and implausible distribution of changes in T_s (IPSL-CM5A-LR). HadGEM2-ES is the most plausible forcing, with globally a peak and decline behaviour leading to overshooting of 1.5°C and over GrIS a slight recovery

10 of SMB towards values of about half the present day SMB. We find sea level to rise for HadGEM2-ES by 71 mm by 2100 and 189 mm by 2300. Simulated an observed sea level rise 2002–2014 is of the same magnitude, but with a temporal lag to be at least five years (HadGEM2-ES). By end of 22nd century sea level contribution is still 0.46 mm a⁻¹ for HadGEM2-ES. Hence, even a RCP2.6 peak and decline scenario will lead to significant changes of GrIS including elevation changes up to 100 m and

15 mass loss are not yet represented by the model, but are considerably larger than other studies.

Copyright statement. We agree to the copyright statements given on the webpage of ESD. The figures within the manuscript are produced by the authors and have not been published by the authors or others in other journals.

1 Introduction

Within the past decade the Greenland ice sheet (GrIS) has contributed in the past decade by about 20% to sea level rise

20 (Rietbroek et al., 2016). The mass loss of GrIS comprises two main contributions: acceleration of outlet glaciers and changes in the surface mass balance. In the past decades these changes in surface mass balance contributed to about 60%, whereas 40% is attributed to increasing discharge (van den Broeke et al., 2016). Obviously the question arises which impact the GrIS



will have in the next decades and centuries. The Paris Agreement during COP21, engaged scientists to assess 'the impacts of global warming of 1.5°C above pre-industrial levels and related global greenhouse gas emission pathway', which is the aim of this study. While the different Representative Concentration Pathways (RCP, Moss et al., 2010) are leading to 1.5°C or 2.0°C global warming at 2100, the global temperature change over time varies considerably between different global circulation models (GCM). Whereas some models are not passing the limit of global warming before 2100, other scenarios cross this limit and exhibit subsequent cooling (Frieler et al., 2016). This effect of returning to below 1.5°C was termed as a potential overshoot (Rogelj et al., 2015). This overshooting could have a considerable impact on ice sheet mass loss and it is currently unclear, how fast GrIS could react to cooling. In order to study this response, we perform simulations in which an ice sheet model is used to simulate the change in ice sheet volume and ice velocities, as response to ice surface temperature and surface mass balance. As these two forcing fields are not a direct output of an atmospheric model we use a surface energy balance model of intermediate complexity to obtain ice surface temperature and surface mass balance. The disadvantage of this type of uncoupled or time slice simulations is the missing response of the atmospheric forcing to ice sheet elevation change, which we aim to overcome by applying corrections to both temperature and surface mass balance. Aiming at covering higher-order physics within the ice sheet model, high spatial resolution in the area of outlet glaciers is required and hence we run the ice sheet model here stand-alone and apply corrections of the atmospheric forcing fields according to the simulated elevation change. The advantage of this approach, is the computational costs, allowing for reasonably high spatial and temporal resolution of the ice sheet model, required for higher-order physics and for capturing the dynamic response of the ice sheet.

For modelling the flow dynamics and future evolution of the GrIS, we apply the thermo-mechanical coupled Ice Sheet System Model (ISSM, Larour et al., 2012). The model is forced with anomalies for temperature and surface mass balance derived from different GCM data from the CMIP5 RCP2.6 scenario provided from the ISIMIP2b project (Frieler et al., 2016). The surface energy balance model SEMIC (Krapp et al., 2017) is applied in order to obtain these anomalies from the GCM data.

2 Model setup

2.1 Ice flow model

Three-dimensional dynamic variables (velocity, pressure, enthalpy) of the GrIS are approximated using the finite-element Ice Sheet System Model. ISSM uses an incompressible non-Newtonian constitutive relation with viscosity dependent on temperature, microscopic-water content and strain rate. while neglecting the softening effect of damage or impurities. ISSM is designed to use variable elements ranging from shallow ice approximation to full-Stokes and has also the capability to perform inverse modelling for inferring basal sliding parameters. The model has been applied successfully to both large ice sheets in the past (Bindschadler et al., 2013; Nowicki et al., 2013; Goelzer et al., 2017) and is also used for studies of individual drainage basins of Greenland, e.g. the North East Greenland Ice Stream (Schlegel et al., 2013), Jakobshavn Isbræ (Bondzio et al., 2016, 2017) and Store Glacier (Morlighem et al., 2016).



Beside the balance equations, ISSM is specified with kinematic boundary conditions at the upper and lower boundary of the ice sheet. The upper boundary incorporates the surface mass balance and with that the climatic forcing, while the base of the ice is specified as both impenetrable with the bedrock and in balance with the rate of melting. Within this study the basal melt rate is not a focus and hence we neither perform sensitivity tests to sliding nor change the basal melt underneath floating tongues or vertical calving fronts of tidewater glaciers. The basal melt rate below ice shelves is parameterised with a Beckmann-Goosse relationship (Beckmann and Goosse, 2003). The unknown melt-factor is roughly tuned such that melting rates corresponds to literature values (e.g. Wilson et al., 2017). At the grounded ice melting occurs due to basal frictional heating and the difference in heat flux at the ice/bed interface.

At the ice base sliding is allowed everywhere and the basal drag, τ_b , is written using Coulomb friction:

$$\tau_b = -k^2 N \mathbf{v}_b, \quad (1)$$

where \mathbf{v}_b is the basal velocity vector tangential to the glacier base and k^2 a constant. The effective pressure is defined as $N = \rho_i g H + \rho_w g h_b$, where H is the ice thickness, h_b the glacier base and $\rho_i = 910 \text{ kg m}^{-3}$, $\rho_w = 1028 \text{ kg m}^{-3}$ the densities for ice and sea water, respectively. We apply water pressure at marine terminating glaciers and observed surface velocities (Rignot and Mouginot, 2012) at land terminating glaciers. A stress-free boundary condition is imposed at the ice/air interface.

Geothermal heat flows into the ice in contact with bedrock (Greve, 2005, scenario hf_pmod2) and adjust dynamically to the thermal state of the base (Aschwanden et al., 2012; Kleiner et al., 2015). The ice surface temperature includes Dirichlet conditions from the atmospheric forcing explained below.

For all simulations, the ice front is fixed in time, and a minimum ice thickness of 10 m is applied. This implies that calving exactly compensate the outflow through the margins and initially glaciated points are not allowed to become ice-free. However, regions that reach this minimum thickness are assumed to retreat. The grounding line is allowed to evolve freely according to the sub-grid parameterization, which tracks the grounding line position within the element (Seroussi et al., 2014).

Model calculations are performed on a horizontally unstructured grid with a higher resolution, l_{\min} , in fast flow regions and coarser resolution, l_{\max} in the interior. The vertical discretisation comprises 15 layers refined towards the base where shearing is dominant. See Table 1 for statistics of the different meshes used. Note that mesh sequence 1-3 are only used during initialization while mesh sequence 4 is used for both initialization and the projections presented below. Velocity, enthalpy and geometry fields are computed on each vertex of the mesh using piecewise-linear finite elements. The Courant-Friedrichs-Lewy condition (Courant et al., 1928) dictates a time step of 0.025 years for mesh sequence 4. Using the AWI cluster Cray-CS 400 computer, a simulation with an integration time of 340 years requires ≈ 8 hours on 16 nodes comprised of 36 CPUs.

2.2 Initial state

Future projections of ice sheet evolution first require the determination of the initial state. Different methods are currently used to initialize ice sheets and it has been shown, that the initial state is crucial for projections of ice dynamics (Bindschadler et al., 2013; Nowicki et al., 2013; Goelzer et al., 2017). The recent initMIP-GrIS intercomparison effort (Goelzer et al., 2017) focusses on the different initialization techniques applied in the ice flow modelling community and found none of them is the



Table 1. Mesh Statistics.

mesh sequence	l_{\min} (km)	l_{\max} (km)	number of elements	integration time in thermal spin-up (kyr)
1	15	50	117 586	125
2	5	50	192 220	125
3	2.5	35	272 650	25
4	1	20	574 056	15

method of choice in terms of a good match to observations or a long term continuity. All methods are suitable for modelling the projections of the GrIS planned within CMIP6 (Nowicki et al., 2016) phase on time scales up to a few hundred years. However, while inverse modelling is well established for estimating basal properties, the temperature field is difficult to constrain without performing an interglacial spin-up. Furthermore, the thermo-mechanically coupled problem is sensitive to temperature.

5 In our initialization approach the ice sheet geometry is initialized over 50 years using zero sliding and constant temperature to avoid spurious noise. The temperature spin-up is then performed using this time-invariant geometry forced with paleo climatic conditions starting 125 kyr before present and up to the year 1960. During the subsequent basal-friction inversion, the ice rheology is kept constant using the enthalpy field from the end of the temperature spin-up. As the computational expensive higher-order approximation to Stokes flow is employed, mesh refinements are made during the whole initialization procedure
10 (see Table 1). Each mesh sequence spin-up is run for \approx 125 kyr, 125 kyr, 25 kyr and 15 kyr, respectively, and updated with the basal-friction coefficient from the previous mesh sequence. The mesh sequencing reduces the expense of initialization and produces a sufficiently consistent result in terms of velocity and enthalpy. The final solution on mesh sequence 4 at year 1960 of this procedure is used as initial state for all projections presented below.

Please note, that similar results from this procedure have been submitted to the ISMIP6 initMIP-Greenland effort (Goelzer
15 et al., 2017), but the simulations were run with the geothermal flux distribution by Shapiro and Ritzwoller (2004) and additionally with a time independent climate forcing representing present-day conditions. However, by using the modified heat-flux distribution by Greve (2005) we found a generally better agreement to measured basal temperatures at ice core locations (Table 2).

2.3 Input data

20 The present-day ice sheet geometry is taken from the mass-conserving bed from BedMachine Greenland (Morlighem et al., 2014). Observed horizontal surface velocities (Rignot and Mouginot, 2012) are assimilated to infer the basal friction coefficient. While the geothermal flux distribution is taken from Greve (2005, scenario hf_pmod2), the present day surface temperature based on the RACMO2 product (Ettema et al., 2009) and the surface temperature anomaly for the last 125 kyr is based on the GRIP surface temperature, T_s , history derived from the $\Delta^{18}O$ record (Dansgaard et al., 1993). Present day surface temperature



Table 2. Simulated (T_{sim}) and observed basal temperatures (T_{obs}) at ice-core locations GRIP, NorthGRIP, Camp Century, Dye3 and East-GRIP. Climate forcing: pd-cl = present day climate, p-cl = paleo climate. Geothermal flux: Gr = Greve (2005), SR = Shapiro and Ritzwoller (2004).

	T_{obs} (°C)	T_{sim} (°C) pd-cl, SR	T_{sim} (°C) pd-cl, Gr	T_{sim} (°C) p-cl, SR	T_{sim} (°C) p-cl, Gr
Camp Century ^a	-13.00	-12.55	-11.79	-14.11	-13.34
NGRIP ^b	-2.40	-16.76	0.00	-22.29	0.00
GRIP ^c	-8.56	-20.92	-18.91	-21.29	-18.39
Dye3 ^d	-13.22	0.00	-8.41	0.00	-8.49
EeastGRIP	?	-2.34	0.00	-14.15	0.00

^aGundestrup et al. (1993) , ^bDahl-Jensen et al. (2003) , ^cDansgaard et al. (1993), Dahl-Jensen et al. (1998),

^dGundestrup and Hansen (2003)

and paleo surface temperature anomaly are taken from the SeaRISE webpage¹. Input data for the surface mass balance is described in the next section.

2.4 Atmospheric forcing

As described above, we aim at using respective output fields (consisting of incoming shortwave radiation SW^{\downarrow} , longwave radiation LW^{\downarrow} , near-surface air temperature T_a , surface wind speed u_s , near-surface specific humidity q_a , surface air pressure p_s , snowfall rate P_s , and rainfall rate P_r) of different GCMs to derive from global models the respective surface temperature T_s , of the ice sheet and the surface mass balance SMB, as GCMs typically do not provide these ice sheet specific quantities. The GCM output was provided and prepared by the ISIMIP2b project following a strict simulation protocol. Here we targeted in particular peak and decline scenarios, temporarily exceeding a given temperature limit of global warming to 2.0°C or even 1.5°C by the end of 2100 (Frieler et al., 2016). Three different GCMs were used in our study: IPSL-CM5A-LR, MIROC5 and HadGEM2-ES. Figure 1a displays the temporal evolution of the annual global mean near-surface temperature T_a , for those GCMs for the historical simulation up to 2005 continued with the RCP2.6 simulation up to 2300. In order to determine the beginning of overshoot and the onset of cooling we extract characteristic dates in global warming and warming above GrIS. HadGEM2-ES produces a global temperature rise of more than 1.5°C by 2021; MIROC5 reaches this level by 2028, while IPSL-CM5A-LR by 2009. IPSL-CM5A-LR is the only GCM that represents any cooling below that limit by 2300, while MIROC5 oscillates around the limit from the 2090s onward. HadGEM2-ES is approaching 1.5°C towards 2170, while remaining slightly above the limit until 2300.

The enhanced increase in global mean air temperature over polar areas has been termed polar amplification. The factor between temperature increase over Greenland compared to the global temperature increase might be as high as 1.8 to 3.3 (IPCC, 2013). Temperatures are rising in Greenland above 1.5°C earlier and exceeding a much higher warming value, representing

¹http://websrv.cs.umt.edu/isis/index.php/Present_Day_Greenland



the effect of the polar amplification (Fig. 1b and 2). Tedesco et al. (2016) demonstrated that this may have consequences on surface melt and run-off in extreme melt years. The three GCMs used in this study represent this trend to differing extents. While HadGEM2-ES and IPSL-CM5A-LR are leading by relatively similar factors (warming up to 5°C relative to 1661–1860), MIROC5 reveals a considerably lower polar amplification (up to 3°C relative to 1661–1860). HadGEM2-ES and MIROC5 exhibit a warming of 1.5°C by 2005, while IPSL-CM5A-LR is also crossing the limit as early as 1995. Both HadGEM2-ES and IPSL-CM5A-LR show no decades until 2300 when the annual mean near-surface air temperature of GrIS is falling below 1.5°C warming relative to 1661–1860, whereas MIROC5 is reaching this value by 2110. A striking feature is the higher variability compared to the global mean values.

Summarizing, in terms of global annual mean near-surface temperature evolution MIROC5 represents the lower bound of our global forcings and IPSL-CM5A-LR represents the upper bound. As the mechanisms creating the polar amplification may be represented to different levels in the GCMs, this trend might be different across the GrIS. While MIROC5 is also across the GrIS the lower bound, highest near-surface temperatures are found for HadGEM2-ES. In terms of overshooting scenarios, HadGEM2-ES represents this behaviour best for overshooting 1.5°C, while IPSL-CM5A-LR rather represents an overshooting of 2°C for about 160 years from 2040 onwards.

To derive ice sheet specific quantities, we use the Surface Energy balance Model of Intermediate Complexity (SEMIC) as developed and applied to the GrIS by Krapp et al. (2017). These authors perform a particle-swarm optimization to calibrate model parameters and validate them against the regional climate model MAR. Due to the fact that Krapp et al. (2017) performed calibration over the GrIS, we adopt the parameters presented in their analysis here. However, we choose a more sophisticated albedo parameterization than was described by Krapp et al. (2017) that is dependent on the actual melt rate (Denby and Greuell, 2000). This reflects the alteration of snow-surface properties by metamorphosis of the snow as function of air temperature. SEMIC is driven by the daily input of the GCMs while the output is a cumulative surface mass balance and a mean surface temperature over each year.

Since the GCM and the ISSM are run on a different resolution, a downscaling procedure is applied to the atmospheric forcing fields. First the atmospheric fields are conservatively interpolated from the GCM grid onto a regular high resolution 0.05° grid. We run the SEMIC model on a regular high resolution 0.05° grid, but the output fields are subsequently conservatively interpolated on the unstructured ISSM grid.

To account for the difference in ice sheet surface topography between GCMs and ISSM, we initially perform corrections for several quantities denoted by $(\cdot)^{\text{cor}}$, while the variables are named according to the SEMIC convention. We basically following the suggested corrections by Vizcaíno et al. (2010)

$$(\cdot)^{\text{cor}} = (h_s^{\text{ISSM-pd}} - h_s^{\text{GCM}})\gamma_{(\cdot)}, \quad (2)$$

with the lapse rates $\gamma_{(\cdot)}$ shown in Table 3 and $h_s^{\text{ISSM-pd}}$ the present-day surface elevation. The surface pressure is not corrected. Subsequently, SEMIC computes the ice-surface temperature T_s and the surface mass balance SMB based on these corrected input values. Furthermore, we apply a dynamic correction to the SMB (SMB_{dyn}) in which we account for the effect of the



Table 3. Lapse rates and height-desertification relationship for initial corrections of GCM output fields near-surface air temperature T_a , precipitation of snow P_s , precipitation of rain P_r , and downward longwave radiation LW^\downarrow used as input for SEMIC. Here, $h^{\text{ref}} = 2000$ m and $\gamma_p = -0.6931 \text{ km}^{-1}$ is the desertification coefficient.

variable	lapse rate γ and desertification relationship	reference
T_a	0.74K/100 m	Erokhina et al. (2017)
LW^\downarrow	2.9 W m^{-2}	Vizcaíno et al. (2010)
P_s, P_r	$\exp(\gamma_p [\max(h_s^{\text{ISSM-pd}}, h^{\text{ref}}) - h^{\text{ref}}]) \quad \forall \quad h_s^{\text{GCM}} \leq h^{\text{ref}}$	Vizcaíno et al. (2010)
P_s, P_r	$\exp(\gamma_p [\max(h_s^{\text{ISSM-pd}}, h^{\text{ref}}) - h_s^{\text{GCM}}]) \quad \forall \quad h_s^{\text{GCM}} > h^{\text{ref}}$	Vizcaíno et al. (2010)

elevation change during the simulations (see below). This correction is applied within ISSM and to the surface mass balance term only.

2.4.1 Atmospheric forcing of future scenarios

The output fields (SMB and T_s) from the SEMIC model are not directly used to force the ISSM. Although the initial state of the ISSM matches the current observations (both ice sheet geometry and surface velocities) very well and the unknown parameters are well constrained due to the data assimilation, usually a fixed initial ice sheet causes a model drift when imposing the ice thickness equation. This is a result from using an ice sheet that is not in perfect equilibrium with the applied SMB and ice flux divergence.

The fixed ice sheet approach during the initialization makes it possible to use forcing data from high resolution climate models that were run on the same ice sheet mask. As a reference SMB field we relied on the downscaled RACMO2.3 product (Noël et al., 2016) whereby a model output was averaged for the time period 1960–1990, denoted $\overline{\text{SMB}}(1960 - 1990)_{\text{RACMO}}$. When using the SMB fields from SEMIC directly, the model drift is much larger compared to using RACMO2.3 SMB (not shown here).

An initial unforced relaxation run from 1960 to 2060 demonstrate the effect of model drift (black line in Fig. 7). Once the ice sheet is released from its fixed topography, it gains of about 3% of its initial volume, which is typical for ice sheet models that are based on data assimilation. We utilize the local ice thickness imbalance from the relaxation run and add the resulting $\partial H / \partial t$ as a surface mass balance correction, $\text{SMB}_{\text{corr}}(x, y, t)$, for the further runs. In doing so, the subsequently performed control run with the imposed correction shows, that the model drift could be reduced by a factor about 0.6 at 2060 (grey line in Fig. 7).

In order to account for the future climate forcing we calculate anomalies from the SEMIC output that were added on the reference SMB field and SMB correction field. The SMB that is used as future climate forcing read as

$$\text{SMB}(x, y, t) = \overline{\text{SMB}}_{\text{RACMO}}^{(1960-1990)}(x, y) + \Delta \text{SMB}(x, y, t) + \text{SMB}_{\text{corr}}(x, y, t), \quad (3)$$



with the anomaly defined as

$$\Delta\text{SMB}(x, y, t) = \text{SMB}_{\text{SEMIC}}(x, y, t) - \overline{\text{SMB}_{\text{SEMIC}}^{(1960-1990)}}(x, y), \quad (4)$$

where $t=\{1960, 1961, \dots, 2299\}$ and $\text{GCM}=\{\text{HadGEM2-ES, IPSL-CM5A-LR, MIROC5}\}$. Note that the historical scenario is run from 1960–2005 and the RCP2.6 scenario from 2006–2299 (Frieler et al., 2016). The same equations hold for the ice temperature imposed on the ice-surface without a correction term. By doing so, the unforced control experiment produces identical behaviour for each GCM. Results for future projection depend only on the atmospheric GCM input, or similarly SEMIC output, and therefore the results can be compared quantitatively.

2.4.2 Dynamic surface mass balance parameterization

The GCM data from the ISIMIP2b simulation protocol were bias corrected onto the regular 0.5° EWEMBI grid (Frieler et al., 2016), where the surface elevation of the ice sheet is fixed in time. In order to account for ongoing height changes between the ISSM surface and the GCM surface we rely on the dynamic SMB parameterization by Edwards et al. (2014a, b) and previously applied by Goelzer et al. (2013). This parameterization assumes that the effect of SMB trends follow a linear relationship

$$\text{SMB}_{\text{dyn}}(x, y, t) = \text{SMB}_{\text{fix}}(x, y, t) + b_i(h(x, y, t) - h_{\text{fix}}(x, y)), \quad (5)$$

where $\text{SMB}_{\text{dyn}}(x, y, t)$ and $\text{SMB}_{\text{fix}}(x, y, t)$ are the SMB values with and without taking height changes into account, respectively ($\text{SMB}_{\text{fix}}(x, y, t)$ is equal to $\text{SMB}(x, y, t)$ in Eq. 3). The surface elevation changes are taken from the ISSM elevation, $h(x, y, t)$ while running the simulation and a reference elevation $h_{\text{fix}}(x, y)$, the present-day surface provided by the BedMachine Greenland dataset (Morlighem et al., 2014).

In this parameterization the SMB gradient b_i , is dependent of both location and sign. It can take four values and a separation is made on the location relative to 77°N and on the sign of the SMB. This separates regions of largely different sensitivity, namely the ablation zone with a larger gradient compared to the accumulation zone, and a more sensitive ablation zone in the South compared to the North. While a complete uncertainty analysis is given by Edwards et al. (2014a), only the maximum likelihood gradient set, $\mathbf{b} = (b_p^N, b_n^N, b_p^S, b_n^S)$, is used here:

$$\begin{aligned} b_p^N &= 0.085 \text{ kg m}^{-3} \text{ a}^{-1}, \\ b_n^N &= 0.543 \text{ kg m}^{-3} \text{ a}^{-1}, \\ b_p^S &= 0.063 \text{ kg m}^{-3} \text{ a}^{-1}, \\ b_n^S &= 1.890 \text{ kg m}^{-3} \text{ a}^{-1}, \end{aligned}$$

where the subscripts (p, n) and the superscripts (N, S) indicate the evaluation of the SMB sign and the region separation, respectively.



2.5 Forcing fields

For the different GCMs used we compute ice-surface temperature differences between 2100 and 2000 as a multi-year mean over five years do reduce the high inter-annual variability. Figure 3 displays the resulting fields for areas that remain ice covered by the year 2100. HadGEM2-ES leads to increase temperatures along the northern margins by up to 4°C. By 2100 the Western areas and vast majority of the ice sheet exceed 2°C. The only pronounced warming by 2300 is in the Northwestern regions, while the ice sheet surface temperatures decreases significantly from 2100. IPSL-CM5A-LR reveals a significantly different pattern. This simulation produces pronounced warming in the center and in the Southeast of the ice sheet, while the Northern areas are only moderately warming. The pattern is similar in 2300, with a cooling in the West. The cooling after 2100 is by far less than in HadGEM2-ES. The least warming is found in MIROC5, which even exhibits cooling in the southern areas by about -1°C and +1°C is only reached in 2100 in the North. By 2300 the entire ice sheet experiences warming; however this warming is quite moderate compared to the other two GCMs. The low magnitude of warming compared to global warming let us infer that the mechanisms of polar amplification is not well represented in MIROC5. Concluding, we find the most plausible distribution of surface warming to be those produced by HadGEM2-ES and MIROC5, while only HadGEM2-ES also reaching a plausible magnitude of warming. IPSL-CM5A-LR is spatially and temporally experiencing the greatest warming; however, the distribution does not appear particularly plausible.

Figure 4 presents in a similar fashion the differences in SMB between 2100 and 2000 as as multi-year mean over five years each. The difference in SMB 2100–2000 of HadGEM2-ES indicates a similar pattern to that presented by Krapp et al. (2017) using MAR (Fettweis et al., 2013). Increasing SMB in the Eastern part of the ice sheet with a maximum in the Southern half of the ice sheet is characteristic for 2300-2000 as well as 2100-2000. Both time periods indicate small glacier valleys in the Southeast and Northwest are exhibiting a strong increase in SMB. This effect arises from the time dependent SMB_{corr} which is in the years 2100 or 2300 much smaller than in the year 2000. After 2100, the SMB is reduced, leaving a wide area with differences in SMB of 0.5 m a^{-1} and more. The SMB difference of IPSL-CM5A-LR is showing an extreme pattern, with SMB reduction as well as increase exceeding $\pm 1 \text{ m a}^{-1}$. The SMB gain is concentrated in the center-East and similar for HadGEM2-ES within the glacier valleys in Southeast and Northwest. The trend in ΔSMB is continuing after 2100, with an even wider area experiencing $+1 \text{ m a}^{-1}$ in the high accumulation are in the east, while the North is experiencing less accumulation than in the 21st century. The most astonishing result is the ΔSMB pattern in MIROC5. Increasing SMB along the western and southern margins in contrast to decreasing SMB in the southwest. ΔSMB is be far less in the period 2300–2100, however, the pattern remains. Similar to changes in temperature, we find HadGEM2-ES to be a GCM with most plausible patterns in ΔSMB . A distinct pattern for all GCMs is a pronounced reduction in SMB at the grounding zone of 79°N Glacier and increasing SMB over many glacier valleys in the Southwest and Northeast.

Beside the pattern of the surface mass balance, the magnitude of the mean SMB over Greenland is a quantity of interest. Therefore, we present a time series of SMB as a five year running mean which is computed as mean over the present day ice covered area (Fig. 5). The grey shaded box and black line depicts the range and the mean SMB between 1981–2000 from Polarportal (polarportal.dk) derived from a combination of observations and a weather model for Greenland (Hirlam-



Newsnow). Although our simulated order of magnitude of SMB is broadly consistent with their range, differences more than hundred Gt a^{-1} occur, which is quite large. There appears to be no covariance of SMB over time between the GCMs. Periods of positive accumulation anomalies are not coincident for the three GCMs. However, the drop in SMB after 2000 is present in all three GCMs. Each GCMs indicates decades of strong accumulation anomalies which are compared with mass loss below.

5 IPSL-CM5A-LR is projecting negative SMB for a large number of years; however even MIROC5 is obtaining negative SMB for numerous years and only HadGEM2-ES is exhibiting few years of negative SMB. Despite the strong variability over time, the underlying pattern is a recovery of the SMB to values of about 250 Gt a^{-1} by 2300.

3 Projections

3.1 Present day elevation and velocities

10 Figure 6 displays exemplary the observed and simulated velocities for the year 2000 after a period of forcing with IPSL-CM5A-LR from 1960 onwards. The resulting horizontal velocity field captures all major features well, including the North East Greenland Ice Stream (NEGIS). Outlet glaciers terminating in narrow fjords in the southeastern region are resolved, however, slow moving areas tend to retreat below minimum ice thickness and with that the ice extent in this area is underestimated. This is also true for slow moving regions in the eastern to northeastern areas. In general large outlet glaciers like Kangerdlusuaq,

15 Helheim and Jakobshavn Isbræ reveal lower velocities in their fast termini. In general the glaciers tend to have a wider area of medium velocities further upstream in the catchment. The numerous glaciers in the western region are all well resolved, with the overall trend of underestimating velocities at the termini.

3.2 Mass loss

To convert the simulated volume above floatation into the total amount of global sea level equivalent (SLE) we assume an

20 ocean area of about $3.618 \times 10^8 \text{ km}^2$. Projections of the evolution of SLE of the ice sheet until 2100 and 2300 are shown in Fig. 7. In addition to the projections for different GCMs we present our control run (grey colour). The model drift is leading to a negative contribution to sea level, resulting in rather conservative mass loss estimates, as the drift accounts for -16.2 mm by 2100. All values for sea level contribution are not corrected with the model drift. Figure 7 includes vertical lines which represent the onset of overshooting of 1.5°C (dotted-dashed lines) in the global annual mean near-surface air temperature, as

25 well as crossing of 1.5°C (dashed lines) over GrIS. The evolution of the mass loss is showing distinct behaviours: between 1960–2000 a reduction, a change in trend with a minor increase between 2000–2015 and a steep increase from then on for HadGEM2-ES and IPSL-CM5a-LR; SLE increases for MIROC5 is more gently. The steep rise in SLE for HadGEM2-ES and IPSL-CM5a-LR is linked to the steep reduction in SMB for both models at the same time. The kink of SLE in HadGEM2-ES and IPSL-CM5A-LR around 2050 is caused by a positive SMB anomaly (compare Fig. 5). Also MIROC5 represents this peak

30 in SMB, however slightly later, around 2060. These reductions in SLE are not linked to the end of an overshooting of the global temperature. Similar to this, all short-term drops in the SLE are linked to positive anomalies in SMB. By ~ 2230 the



differences in SMB between the three GCMs is considerably reduced and also the inter-annual variability has decreased. This is linked to the end of overshooting in global temperatures in HadGEM2-ES and IPSL-CM5A-LR. The cumulative SLE does in that time period approach a plateau for MIROC5 and IPSL-CM5A-LR, while for HadGEM2-ES the ice sheet contribution is still increasing. This is potentially an effect of ice dynamics that may be underrepresented with the forcings from MIROC5
5 and IPSL-CM5A-LR.

Forcing the ice sheet with HadGEM2-ES leads to a mass loss that is concentrated in the Western and Southwestern regions of the ice sheet with moderate elevation reduction in the Eastern region and an increase in elevation in the center-North (Fig. 8). IPSL-CM5A-LR forcing is to a gradient pattern with high elevation reduction in the West and increase in ice sheet height in the East. In particular the catchments of Helheim and Kangerdlusuaq glaciers are showing a false trend compared to observations.
10 With a forcing of MIROC5 the pattern of the elevation change is more similar to HadGEM2-ES result with a slight shift of the maximum elevation and a general lower magnitude of elevation change. Compared to HadGEM2-ES the south experience more elevation reduction in the higher elevated parts, whereas HadGEM2-ES is showing a pronounced surface lowering at the coastal margins. In conclusion, the elevation change resulting from HadGEM2-ES appears most plausible in pattern and magnitude. The ice tongues of Petermann, Ryder and 79°N glaciers are in all forcings threatened in their existence, even with
15 the moderate forcing of MIROC5. Kong Christian IX Land vanish nearly entirely in the simulations forced with HadGEM2-ES and also the area in vicinity of the Renland ice cap would become ice free in this projection by 2100. All three GCM forcings lead to a spot of elevation drop in the north around CH Ostensfeld Glacier which is suspicious, as there is no link to any SMB forcing present in this area in all three GCMs. We expect this to be an effect of errors in vertical ice velocities in this area.

The observed sea level contribution between 2002 and 2014 is 0.73 mm a^{-1} (Rietbroek et al., 2016), while we find in the
20 same period only 0.21 mm a^{-1} for HadGEM2-ES, as low as 0.13 mm a^{-1} for IPSL-CM5A-LR and largest for MIROC5 with 0.26 mm a^{-1} . In order to assess with which temporal lag our simulations are reaching the observed value, we present in Fig. 9 mean values of a similar period of time. HadGEM2-ES reaches the observed values 5-6 years later, IPSL-CM5A-LR about 9 years and MIROC5 about 33-35 years. In general the comparison with observations obey the drawback that the emission scenarios are based on emissions cuts that have not yet been fully set into practise. Thus the observations show a response of
25 the ice sheet to an emission scenario that is different to our forcing and this not only due to climate models capabilities, but due to differences in prescribed RCP and real RCP. This would result at least in a temporal lag.

3.3 Acceleration

The response of ice velocities to atmospheric forcing is presented in Fig. 10, where the change in horizontal surface velocities is shown for all scenarios as a difference between 2100–2000 and 2300–2000 (each as five year mean). All GCM forcings
30 lead to deceleration of the glaciers in the west and southeast, while glaciers in the north and northeast accelerate. By 2300 HadGEM2-ES and IPSL-CM5A-LR project a slight increase in flow speeds in the higher elevated areas indicating a shift in future ice divide positions. A common pattern among all GCM forcings is an acceleration of NEGIS and in particular 79°N, ranging into both branches of this glacier by 2300. Also Ryder glacier and Hagen Bræ experience among all simulations an acceleration.



Acceleration of Jakobshavn Isbræ is present in our simulations, however, not to the extent of the observations (Joughin et al., 2014). This is due to the lack of forcing with calving rates in our simulations, which has been key for reproducing the observed acceleration and retreat in Bondzio et al. (2017).

5 Helheim Glacier experience in nearly all simulations an acceleration in its main trunk, while its upstream catchment is decelerating. The glaciers in the southwest and Kangerdlussaq Glacier are decelerating in our projections. This is corresponding to elevation increase in the south-east. We suggest this to be an effect of the SMB in this area, which appears to be too large. Also the synthetic SMB is quite high in this area undermining this to be an effect of overestimated SMB. Helheim Glacier acceleration is thus likely a dynamic response by its special bed topography which is not levelled out by artificially high SMB. Also in the western areas, we find nearby glaciers altering between acceleration and deceleration that indicates their response
10 to geometric settings at their base. This is also exemplifying that our model is able to resolve the glacier valleys well.

Our estimated results of a sea level contribution are substantially higher than results by Fürst et al. (2015). They performed a comprehensive ensemble study for a suite of 10 atmosphere and ocean general circulation models (HadGEM2-ES, IPSL-CM5A-LR and MIROC5 included) and four representative concentration pathway scenarios. For the RCP2.6 scenario they estimate a sea level contribution of $42.3 \pm 18.0 \text{ mm a}^{-1}$ by 2100 and $88.2 \pm 44.8 \text{ mm a}^{-1}$ by 2300. At least for IPSL-CM5A-LR
15 and MIRCOC5 the abated contribution with the warming peak in this century is consistent. Although, they have an future ocean forcing included they estimate a lower contribution. In fact, the effect of the ocean forcing is not dominant and tend to decrease with a shrinking ice sheet that loose the contact to the ocean. A major difference between our models is certainly the resolution, as our model does resolve the outlet glaciers reasonably well. However, this does so far not contribute too strongly, as our setup does not apply particular strong ocean forcings and lacks any additional lubrication effects.

20 The question why our values are substantially higher needs to be assessed for two different aspects, one is the models sensitivity, the other one is the difference in forcing. Compared to other models that participate in the initMIP (Goelzer et al., 2017), our model is not in general on the higher end of the spectrum of estimated mass loss. We have conducted SeaRISE experiments similar to Bindschadler et al. (2013) (not shown here), which showed us that we are among the models with higher sensitivity to climate forcing. Together with selecting RCP2.6 scenarios with an pronounced overshoot on purpose, this
25 is very likely to lead to higher values for mass loss.

4 Conclusions

We have applied three different GCM (HadGEM2-ES, IPSL-CM5A-LR, MIROC5) forcings for RCP2.6 to estimate the response of GrIS to overshooting scenarios. Despite all three GCMs are based on RCP2.6, their variation is considerably large. Polar amplification causes a near-surface air temperature increase over Greenland by a factor of ≈ 2.4 and 2 in HadGEM2-ES
30 and IPSL-CM5A-LR, respectively. MIROC5 reveals nearly no polar amplification. Sea level rise is ranging in our simulations from 46 to 71 mm by 2100 and 114 to 189 mm by 2300. The most plausible forcing HadGEM2-ES leads to 71 mm by 2100 and 189 mm by 2300. Surface elevation drops in the southwest by up to 100 m and leads also to considerable retreat along the eastern coast, with leaving Kong Christian IX Land nearly ice free by 2300. The ice tongues of 79°N glacier, Ryder and



Petermann glacier are lost already by 2100. Acceleration of NEGIS, Helheim Glacier and Jakobshavn Isbræ is represented in our model, but potentially underestimated due to the following drawbacks of our study: (i) retreat of glaciers due to oceanic forcing (melt at vertical cliffs and/or calving rates) is not included so far, (ii) model drift is still quite large, resulting from the switching between spin-up to RCP forcings and (iii) seasonality due to lubrication arising from supra-glacial melt water is not included. This limits also the advantageous treatment of the physics in our model setup, meaning that all the benefits from a high-resolution higher order model are not yet contributing to the extent they potentially could. This leads to the conclusion that the projections may serve as a lower bound of the contribution of Greenland to sea level rise under RCP2.6.

Code availability. The ice sheet model ISSM is available at issm.jpl.nasa.gov and not distributed by the authors of this manuscript. SEMIC is available from <https://gitlab.pik-potsdam.de/krapp/semic-project> and not distributed by the authors of this manuscript.

10 *Author contributions.* M.R. conducted the ISSM simulations, coupled SEMIC output to ISSM. M.R. and A.H. designed the study, analysed the results and wrote major parts of the manuscript. K.F. and S.L. selected, prepared and contributed GCM forcings. U.F. has contributed advice on the albedo scheme and checked the GCM input data.

Competing interests. There are no competing interests present.

15 *Acknowledgements.* This work was funded by BMBF under grant EP-GrIS (01LS1603A) and the Helmholtz Alliance Climate Initiative (REKLIM). We acknowledge the technical support given by Mario Krapp (PIK) with SEMIC. We are grateful for the NetCDF interface to SEMIC provided by Paul Gierz (AWI). We would like to thank Vadym Aizinger, Natalja Rakowsky and Malte Thoma for maintaining excellent computing facilities at AWI. We also enthusiastically acknowledge the general support of the ISSM team.



References

- Aschwanden, A., Bueler, E., Khroulev, C., and Blatter, H.: An enthalpy formulation for glaciers and ice sheets, *Journal of Glaciology*, 58, 441–457, <https://doi.org/10.3189/2012JoG11J088>, 2012.
- Beckmann, A. and Goosse, H.: A parameterization of ice shelf–ocean interaction for climate models, *Ocean Modelling*, 5, 157–170, [https://doi.org/10.1016/S1463-5003\(02\)00019-7](https://doi.org/10.1016/S1463-5003(02)00019-7), 2003.
- 5 Bindschadler, R. A., Nowicki, S., Abe-Ouchi, A., Aschwanden, A., Choi, H., Fastook, J., Granzow, G., Greve, R., Gutowski, G., Herzfeld, U., Jackson, C., Johnson, J., Khroulev, C., Levermann, A., Lipscomb, W. H., Martin, M. A., Morlighem, M., Parizek, B. R., Pollard, D., Price, S. F., Ren, D., Saito, F., Sato, T., Seddik, H., Seroussi, H., Takahashi, K., Walker, R., and Wang, W. L.: Ice-sheet model sensitivities to environmental forcing and their use in projecting future sea level (the SeaRISE project), *Journal of Glaciology*, 59, 195–
- 10 224, <https://doi.org/doi:10.3189/2013JoG12J125>, 2013.
- Bondzio, J. H., Seroussi, H., Morlighem, M., Kleiner, T., Rückamp, M., Humbert, A., and Larour, E. Y.: Modelling calving front dynamics using a level-set method: application to Jakobshavn Isbræ, West Greenland, *The Cryosphere*, 10, 497–510, <https://doi.org/10.5194/tc-10-497-2016>, 2016.
- Bondzio, J. H., Morlighem, M., Seroussi, H., Kleiner, T., Rückamp, M., Mouginot, J., Moon, T., Larour, E. Y., and Humbert, A.: The
- 15 mechanisms behind Jakobshavn Isbræ’s acceleration and mass loss: A 3-D thermomechanical model study, *Geophysical Research Letters*, 44, 6252–6260, <https://doi.org/10.1002/2017GL073309>, 2017GL073309, 2017.
- Courant, R., Friedrichs, K., and Lewy, H.: Über die Partiellen Differenzengleichungen der Mathematischen Physik, *Mathematische Annalen*, 100, 32–74, 1928.
- Dahl-Jensen, D., Mosegaard, K., Gundestrup, N., Clow, G. D., Johnsen, S. J., Hansen, A. W., and Balling, N.: Past Temperatures Directly
- 20 from the Greenland Ice Sheet, *Science*, 282, 268–271, <https://doi.org/10.1126/science.282.5387.268>, 1998.
- Dahl-Jensen, D., Gundestrup, N., Gogineni, S., and Miller, H.: Basal melt at NorthGRIP modeled from borehole, ice-core and radio-echo sounder observations, *Annals of Glaciology*, 37, 207–212, 2003.
- Dansgaard, W., Johnsen, S., Clausen, H., Dahl-Jensen, D., Gundestrup, N., Hammer, C., Hvidberg, C., Steffensen, J., Sveinbjörndottir, A., Jouzel, J., and Bond, G.: Evidence for general instability of past climate from a 250-kyr ice-core record, *Nature*, 364, 218–220,
- 25 <https://doi.org/doi:10.1038/364218a0>, 1993.
- Denby, B. and Greuell, W.: The use of bulk and profile methods for determining surface heat fluxes in the presence of glacier winds, *Journal of Glaciology*, 46, 445–452, 2000.
- Edwards, T. L., Fettweis, X., Gagliardini, O., Gillet-Chaulet, F., Goelzer, H., Gregory, J. M., Hoffman, M., Huybrechts, P., Payne, A. J., Perego, M., Price, S., Quiquet, A., and Ritz, C.: Probabilistic parameterisation of the surface mass balance elevation feedback in regional
- 30 climate model simulations of the Greenland ice sheet, *The Cryosphere*, 8, 181–194, <https://doi.org/10.5194/tc-8-181-2014>, 2014a.
- Edwards, T. L., Fettweis, X., Gagliardini, O., Gillet-Chaulet, F., Goelzer, H., Gregory, J. M., Hoffman, M., Huybrechts, P., Payne, A. J., Perego, M., Price, S., Quiquet, A., and Ritz, C.: Effect of uncertainty in surface mass balance elevation feedback on projections of the future sea level contribution of the Greenland ice sheet, *The Cryosphere*, 8, 195–208, <https://doi.org/10.5194/tc-8-195-2014>, 2014b.
- Erokhina, O., Rogozhina, I., Prange, M., Bakker, P., Bernales, J., Paul, A., and Schulz, M.: Dependence of slope lapse rate over the Greenland
- 35 ice sheet on background climate, *Journal of Glaciology*, 63, 568, <https://doi.org/10.1017/jog.2017.10>, 2017.



- Ettema, J., van den Broeke, M. R., van Meijgaard, E., van de Berg, W. J., Bamber, J. L., Box, J. E., and Bales, R. C.: Higher surface mass balance of the Greenland ice sheet revealed by high-resolution climate modeling, *Geophysical Research Letters*, 36, n/a–n/a, <https://doi.org/10.1029/2009GL038110>, 112501, 2009.
- 5 Fettweis, X., Franco, B., Tedesco, M., van Angelen, J. H., Lenaerts, J. T. M., van den Broeke, M. R., and Gallée, H.: Estimating the Greenland ice sheet surface mass balance contribution to future sea level rise using the regional atmospheric climate model MAR, *The Cryosphere*, 7, 469–489, <https://doi.org/10.5194/tc-7-469-2013>, 2013.
- Frieler, K., Betts, R., Burke, E., Ciais, P., Denvil, S., Deryng, D., Ebi, K., Eddy, T., Emanuel, K., Elliott, J., Galbraith, E., Gosling, S. N., Halladay, K., Hattermann, F., Hickler, T., Hinkel, J., Huber, V., Jones, C., Krysanova, V., Lange, S., Lotze, H. K., Lotze-Campen, H., Mengel, M., Mouratiadou, I., Müller Schmied, H., Ostberg, S., Piontek, F., Popp, A., Reyer, C. P. O., Schewe, J., Stevanovic, M., Suzuki, 10 T., Thonicke, K., Tian, H., Tittensor, D. P., Vautard, R., van Vliet, M., Warszawski, L., and Zhao, F.: Assessing the impacts of 1.5 °C global warming – simulation protocol of the Inter-Sectoral Impact Model Intercomparison Project (ISIMIP2b), *Geoscientific Model Development Discussions*, 2016, 1–59, <https://doi.org/10.5194/gmd-2016-229>, 2016.
- Fürst, J. J., Goelzer, H., and Huybrechts, P.: Ice-dynamic projections of the Greenland ice sheet in response to atmospheric and oceanic warming, *The Cryosphere*, 9, 1039–1062, <https://doi.org/10.5194/tc-9-1039-2015>, <https://www.the-cryosphere.net/9/1039/2015/>, 2015.
- 15 Goelzer, H., Huybrechts, P., Fürst, J., Nick, F., Andersen, M., Edwards, T., Fettweis, X., Payne, A., and Shannon, S.: Sensitivity of Greenland Ice Sheet Projections to Model Formulations, *Journal of Glaciology*, 59, 733–749, <https://doi.org/10.3189/2013JG12J182>, 2013.
- Goelzer, H., Nowicki, S., Edwards, T., Beckley, M., Abe-Ouchi, A., Aschwanden, A., Calov, R., Gagliardini, O., Gillet-Chaulet, F., Gollège, N. R., Gregory, J., Greve, R., Humbert, A., Huybrechts, P., Kennedy, J. H., Larour, E., Lipscomb, W. H., Le clec'h, S., Lee, V., Morlighem, M., Pattyn, F., Payne, A. J., Rodehacke, C., Rückamp, M., Saito, F., Schlegel, N., Seroussi, H., Shepherd, A., Sun, S., van de Wal, R., and 20 Ziemen, F. A.: Design and results of the ice sheet model initialisation experiments initMIP-Greenland: an ISMIP6 intercomparison, *The Cryosphere Discussions*, 2017, 1–42, <https://doi.org/10.5194/tc-2017-129>, 2017.
- Greve, R.: Relation of measured basal temperatures and the spatial distribution of the geothermal heat flux for the Greenland ice sheet, *Annals of Glaciology*, 42, 424–432, 2005.
- Gundestrup, N. and Hansen, B.: Bore-hole survey at Dye 3, south Greenland, *Journal of Glaciology*, 30, 282–288, 2003.
- 25 Gundestrup, N., Dahl-Jensen, D., Hansen, B., and Kelty, J.: Bore-hole survey at Camp Century, 1989, *Cold Regions Science and Technology*, 21, 187–193, [https://doi.org/10.1016/0165-232X\(93\)90006-T](https://doi.org/10.1016/0165-232X(93)90006-T), 1993.
- IPCC: Climate Change 2013: The Physical Science Basis. Contribution of Working Group I to the Fifth Assessment Report of the Intergovernmental Panel on Climate Change, Cambridge University Press, Cambridge, United Kingdom and New York, NY, USA, <https://doi.org/10.1017/CBO9781107415324>, www.climatechange2013.org, 2013.
- 30 Joughin, I., Smith, B. E., Shean, D. E., and Floricioiu, D.: Brief Communication: Further summer speedup of Jakobshavn Isbræ, *The Cryosphere*, 8, 209–214, <https://doi.org/10.5194/tc-8-209-2014>, <https://www.the-cryosphere.net/8/209/2014/>, 2014.
- Kleiner, T., Rückamp, M., Bondzio, J. H., and Humbert, A.: Enthalpy benchmark experiments for numerical ice sheet models, *The Cryosphere*, 9, 217–228, <https://doi.org/10.5194/tc-9-217-2015>, 2015.
- Krapp, M., Robinson, A., and Ganopolski, A.: SEMIC: an efficient surface energy and mass balance model applied to the Greenland ice sheet, *The Cryosphere*, 11, 1519–1535, <https://doi.org/10.5194/tc-11-1519-2017>, 2017.
- 35 Larour, E., Seroussi, H., Morlighem, M., and Rignot, E.: Continental scale, high order, high spatial resolution, ice sheet modeling using the Ice Sheet System Model (ISSM), *Journal of Geophysical Research: Earth Surface*, 117, <https://doi.org/10.1029/2011JF002140>, 2012.



- Morlighem, M., Rignot, E., Mouginot, J., Seroussi, H., and Larour, E.: Deeply incised submarine glacial valleys beneath the Greenland ice sheet, *Nature Geoscience*, 7, 418–422, <https://doi.org/10.1038/ngeo2167>, 2014.
- Morlighem, M., Bondzio, J., Seroussi, H., Rignot, E., Larour, E., Humbert, A., and Rebuffi, S.: Modeling of Store Gletscher's calving dynamics, West Greenland, in response to ocean thermal forcing, *Geophysical Research Letters*, 43, 2659–2666, <https://doi.org/10.1002/2016GL067695>, 2016GL067695, 2016.
- 5 Moss, R. H., Edmonds, J. A., Hibbard, K. A., Manning, M. R., Rose, S. K., van Vuuren, D. P., Carter, T. R., Emori, S., Kainuma, M., Kram, T., Meehl, G. A., Mitchell, J. F. B., Nakicenovic, N., Riahi, K., Smith, S. J., Stouffer, R. J., Thomson, A. M., Weyant, J. P., and Wilbanks, T. J.: The next generation of scenarios for climate change research and assessment, *Nature*, 463, 747–756, <http://dx.doi.org/10.1038/nature08823>, 2010.
- 10 Noël, B., van de Berg, W. J., Machguth, H., Lhermitte, S., Howat, I., Fettweis, X., and van den Broeke, M. R.: A daily, 1 km resolution data set of downscaled Greenland ice sheet surface mass balance (1958–2015), *The Cryosphere*, 10, 2361–2377, <https://doi.org/10.5194/tc-10-2361-2016>, 2016.
- Nowicki, S., Bindschadler, R. A., Abe-Ouchi, A., Aschwanden, A., Bueller, E., Choi, H., Fastook, J., Granzow, G., Greve, R., Gutowski, G., Herzfeld, U., Jackson, C., Johnson, J., Khroulev, C., Larour, E., Levermann, A., Lipscomb, W. H., Martin, M. A., Morlighem, M., Parizek, B. R., Pollard, D., Price, S. F., Ren, D., Rignot, E., Saito, F., Sato, T., Seddik, H., Seroussi, H., Takahashi, K., Walker, R., and Wang, W. L.: Insights into spatial sensitivities of ice mass response to environmental change from the SeaRISE ice sheet modeling project II: Greenland, *Journal of Geophysical Research: Earth Surface*, 118, 1025–1044, <https://doi.org/10.1002/jgrf.20076>, 2013.
- 15 Nowicki, S. M. J., Payne, A., Larour, E., Seroussi, H., Goelzer, H., Lipscomb, W., Gregory, J., Abe-Ouchi, A., and Shepherd, A.: Ice Sheet Model Intercomparison Project (ISMIP6) contribution to CMIP6, *Geoscientific Model Development*, 9, 4521–4545, <https://doi.org/10.5194/gmd-9-4521-2016>, 2016.
- 20 Rietbroek, R., Brunnabend, S.-E., Kusche, J., Schröter, J., and Dahle, C.: Revisiting the contemporary sea-level budget on global and regional scales, *Proceedings of the National Academy of Sciences*, 113, 1504–1509, <https://doi.org/10.1073/pnas.1519132113>, 2016.
- Rignot, E. and Mouginot, J.: Ice flow in Greenland for the International Polar Year 2008–2009, *Geophysical Research Letters*, 39, n/a–n/a, <https://doi.org/10.1029/2012GL051634>, 2012.
- 25 Rogelj, J., Luderer, G., Pietzcker, R. C., Kriegler, E., Schaeffer, M., Krey, V., and Riahi, K.: Energy system transformations for limiting end-of-century warming to below 1.5°C, *Nature Clim. Change*, 5, 519–527, <http://dx.doi.org/10.1038/nclimate2572>, 2015.
- Schlegel, N. J., Larour, E., Seroussi, H., Morlighem, M., and Box, J. E.: Decadal-scale sensitivity of Northeast Greenland ice flow to error in a surface mass balance using ISSM, *Journal of Geophysical Research: Earth Surface*, 118, 667–680, <https://doi.org/10.1002/jgrf.20062>, 2013.
- 30 Seroussi, H., Morlighem, M., Larour, E., Rignot, E., and Khazendar, A.: Hydrostatic grounding line parameterization in ice sheet models, *The Cryosphere*, 8, 2075–2087, <https://doi.org/10.5194/tc-8-2075-2014>, 2014.
- Shapiro, N. and Ritzwoller, M.: Inferring surface heat flux distributions guided by a global seismic model: Particular application to Antarctica, *Earth and Planetary Science Letters*, 223, 213–224, <https://doi.org/10.1016/j.epsl.2004.04.011>, 2004.
- Tedesco, M., Mote, T., Fettweis, X., Hanna, E., Jeyaratnam, J., Booth, J. F., Datta, R., and Briggs, K.: Arctic cut-off high drives the poleward shift of a new Greenland melting record, *Nature Communications*, 7, 11 723 EP –, <http://dx.doi.org/10.1038/ncomms11723>, 2016.
- 35 van den Broeke, M. R., Enderlin, E. M., Howat, I. M., Kuipers Munneke, P., Noël, B. P. Y., van de Berg, W. J., van Meijgaard, E., and Wouters, B.: On the recent contribution of the Greenland ice sheet to sea level change, *The Cryosphere*, 10, 1933–1946, <https://doi.org/10.5194/tc-10-1933-2016>, 2016.



Vizcaíno, M., Mikolajewicz, U., Jungclaus, J., and Schurgers, G.: Climate modification by future ice sheet changes and consequences for ice sheet mass balance, *Climate Dynamics*, 34, 301–324, <https://doi.org/10.1007/s00382-009-0591-y>, 2010.

Wilson, N., Straneo, F., and Heimbach, P.: Submarine melt rates and mass balance for Greenland's remaining ice tongues, *The Cryosphere Discussions*, 2017, 1–17, <https://doi.org/10.5194/tc-2017-99>, 2017.

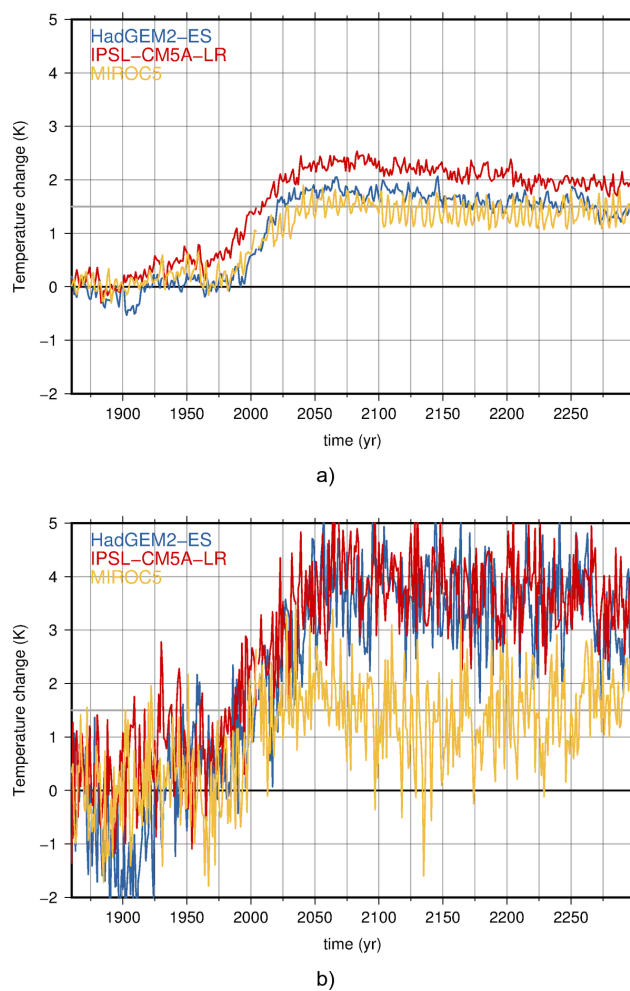


Figure 1. Time series of annual global mean near-surface temperature change a) and over the GrIS b) for all three GCMs relative to 1661–1880.

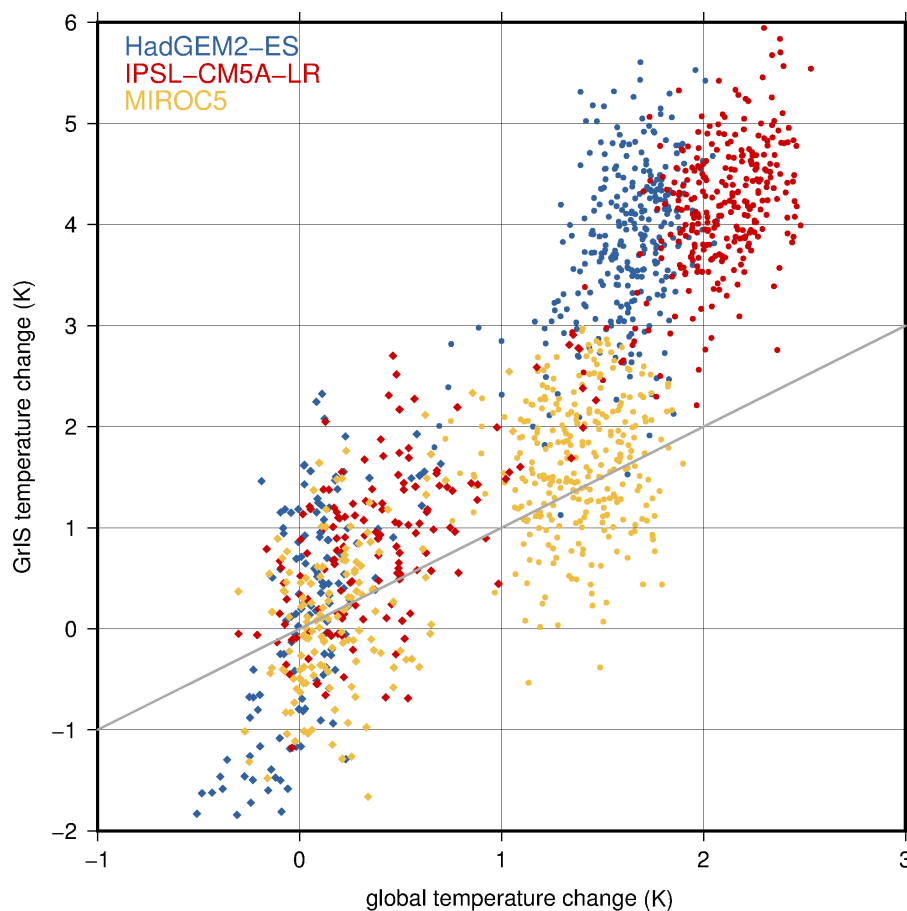


Figure 2. Scatter plot of annual mean near-surface air temperatures over GrIS versus annual global mean near-surface air temperatures. The grey line depicts a linear course.

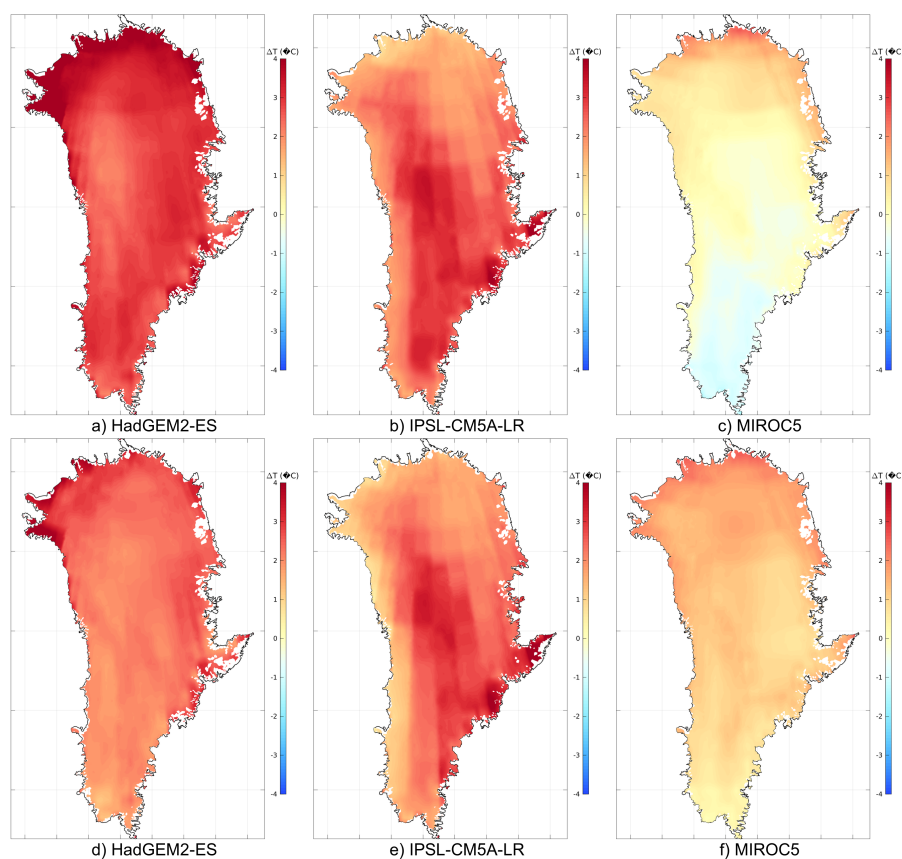


Figure 3. Comparison of multi-year mean surface temperature (T_s) differences between 2100–2000 (top row) and 2300–2000 (bottom row) for (a,d) HadGEM2-ES, (b,e) IPSL-CM5A-LR and (c,f) MIROC5. The black contour line depicts the present-day ice mask.

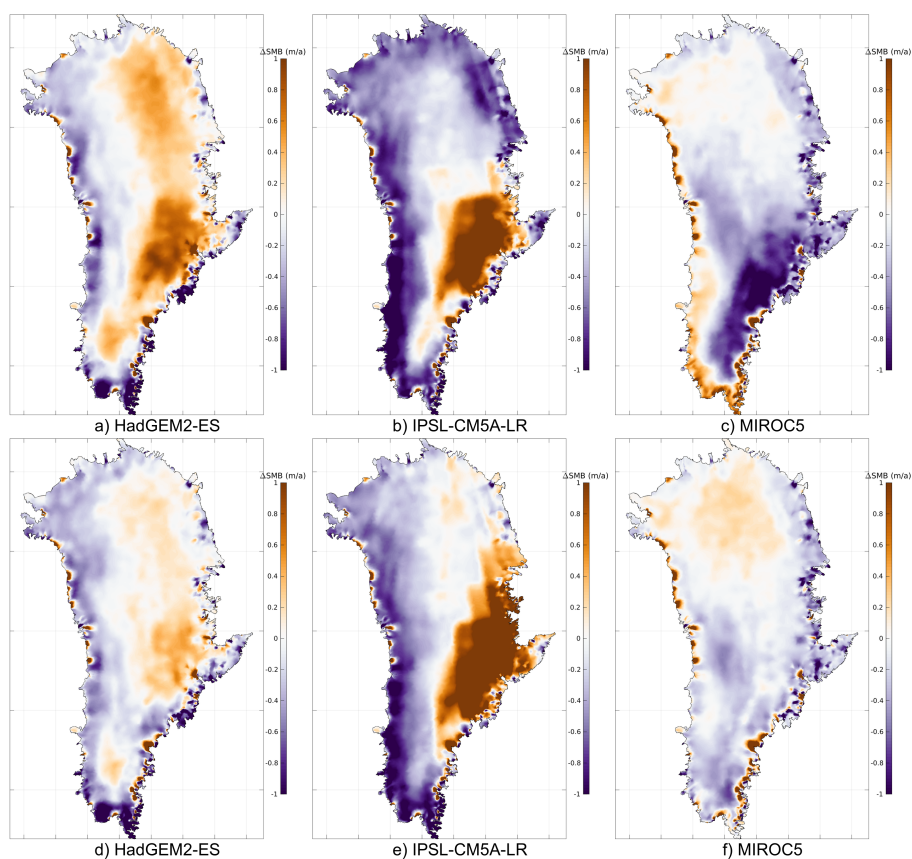


Figure 4. Comparison of multi-year mean surface mass balance (SMB) differences between 2100-2000 (top row) and 2300-2000 (bottom row) for (a,d) HadGEM2-ES, (b,e) IPSL-CM5A-LR and (c,f) MIROC5. The black contour line depicts the present-day ice mask.

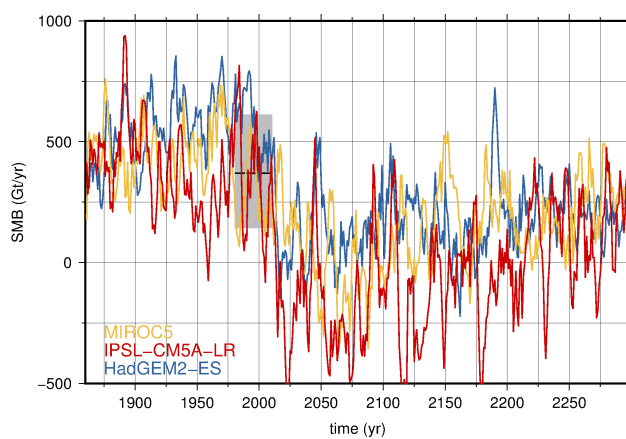


Figure 5. Time series of SMB (five year running mean) according to Eq. 3 for all three GCMs. In grey colour the range and mean of SMB between 1981–2000 from Polarportal is marked (polarportal.dk).

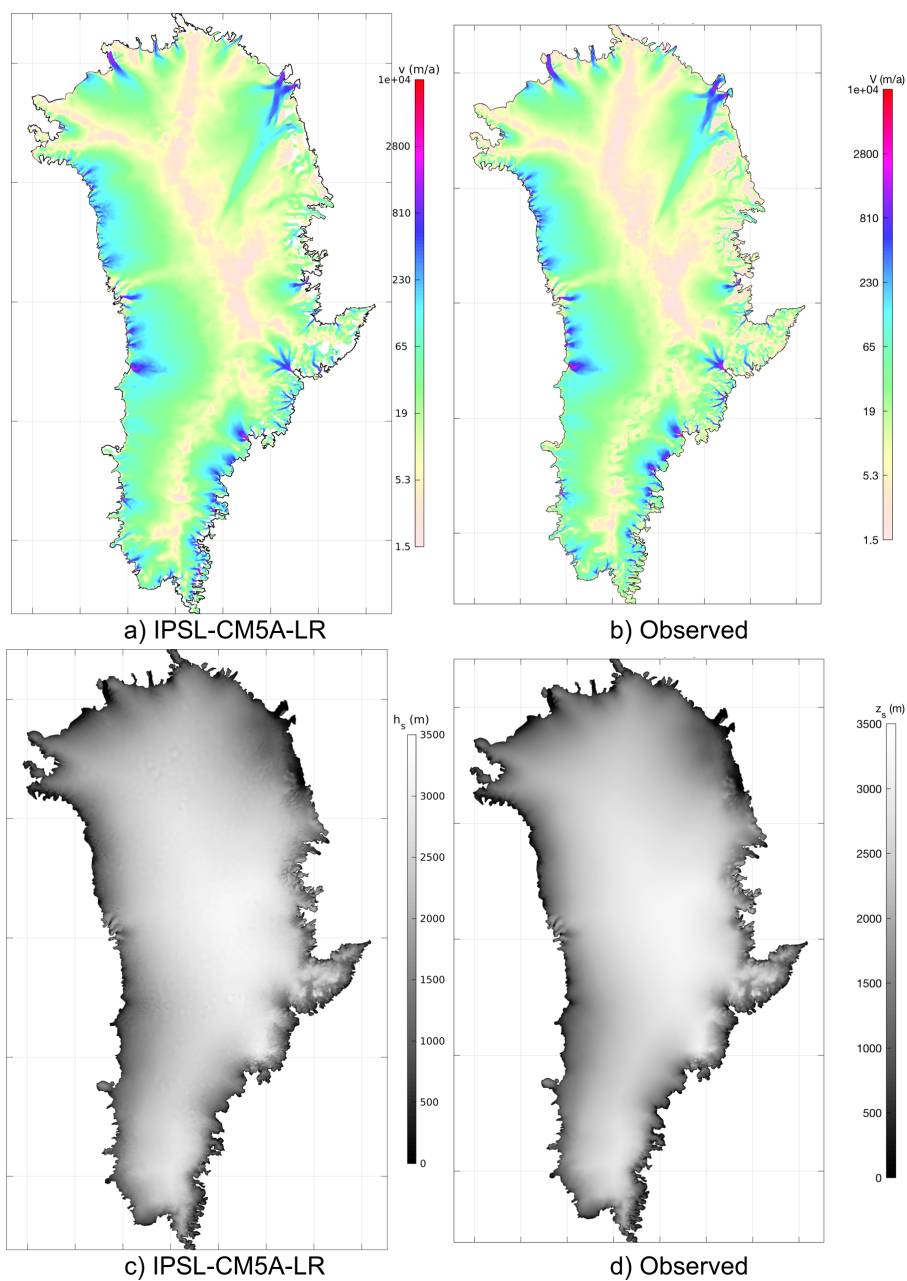


Figure 6. Current state for 2000 using IPSL-CM5A-LR: (a) simulated velocities, (b) observed velocities, (c) simulated surface elevation, (d) observed surface elevation. Observed velocities: Rignot and Mouginot (2012); Observed surface elevation: Morlighem et al. (2014).

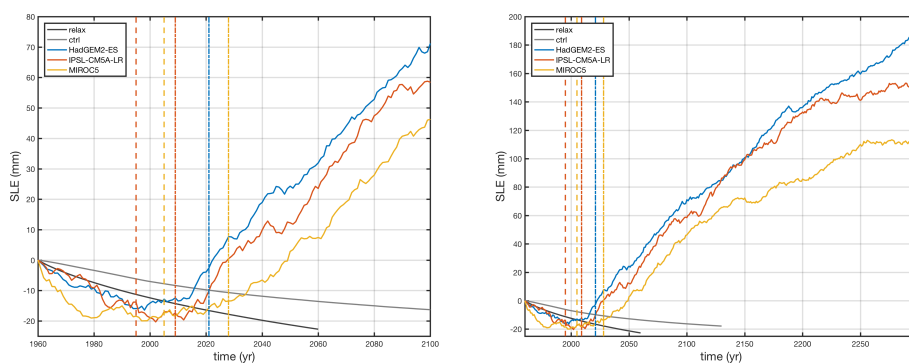


Figure 7. Sea level equivalent until the year 2100 (left panel) and 2300 (right panel) for all GCMs. Additionally the relaxation and control run are shown. The dotted-dashed and dashed lines represent the onset of overshooting 1.5°C in the global mean near-surface air temperature and the corresponding overshoot over GrIS, respectively.

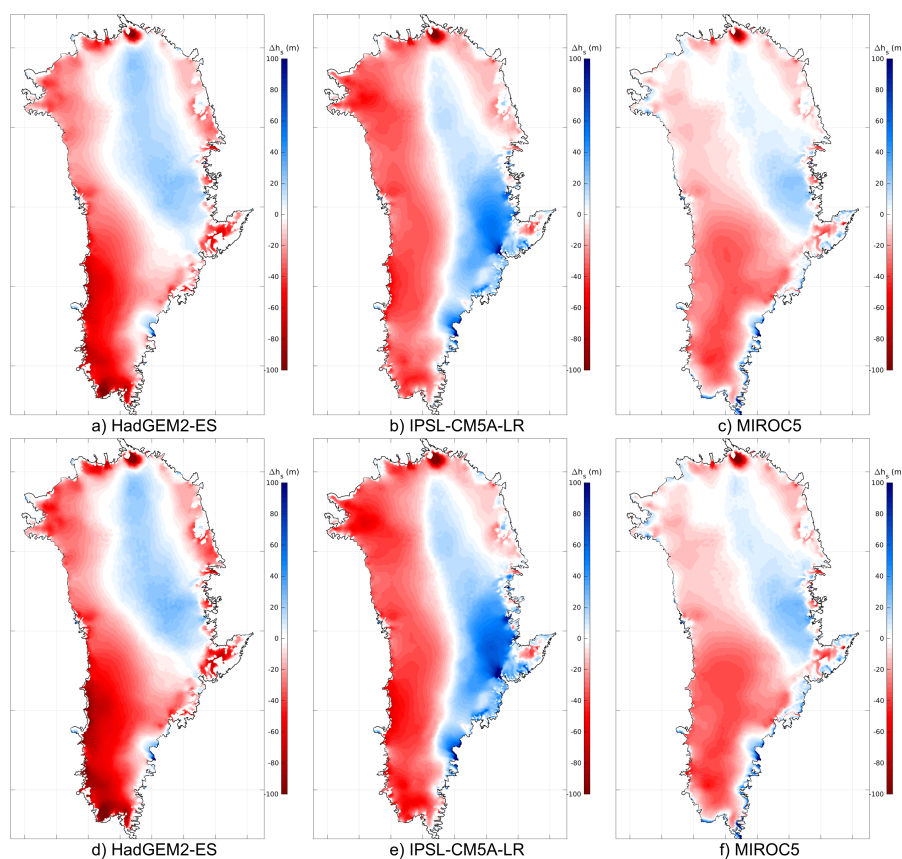


Figure 8. Comparison of multi-year mean surface elevation (h_s) differences between 2100-2000 (top row) and 2300-2000 (bottom row) for (a,d) HadGEM2-ES, (b,e) IPSL-CM5A-LR and (c,f) MIROC5. The black contour line depicts the present-day ice mask.

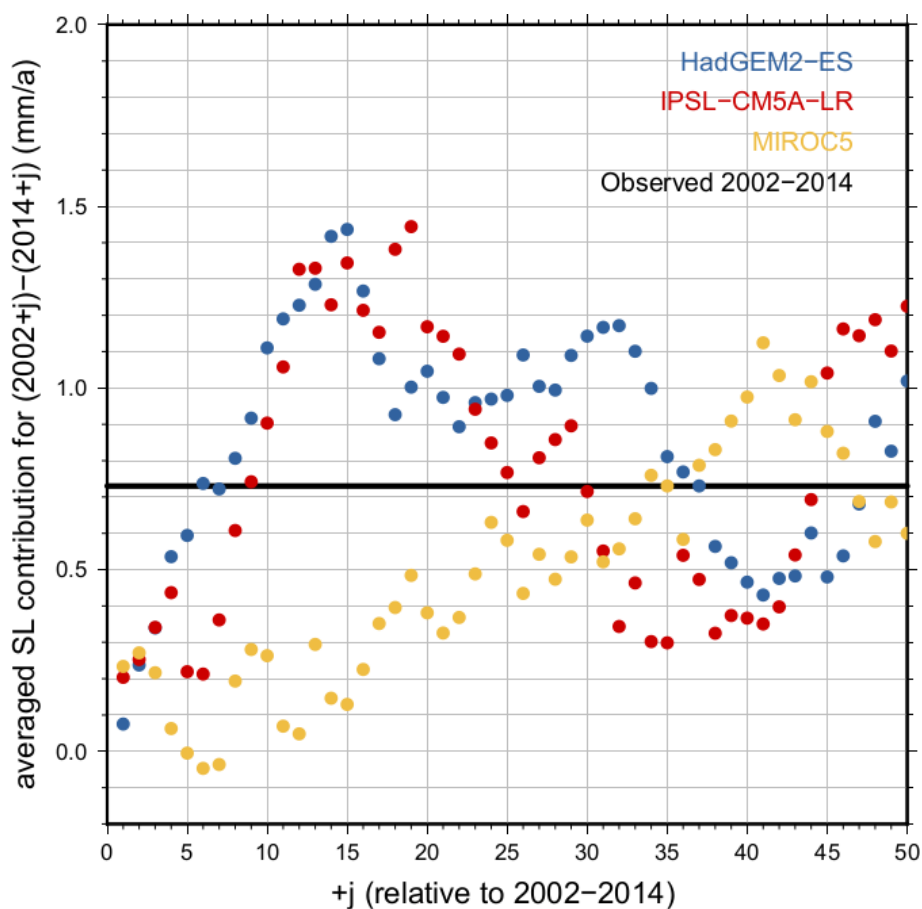


Figure 9. Lag (j) of projected sea level rise per year for three GCMs as mean for a time period similar to the observational period (2002–14). The black line indicates the observed value of 0.73 mm a^{-1} by Rietbroek et al. (2016).

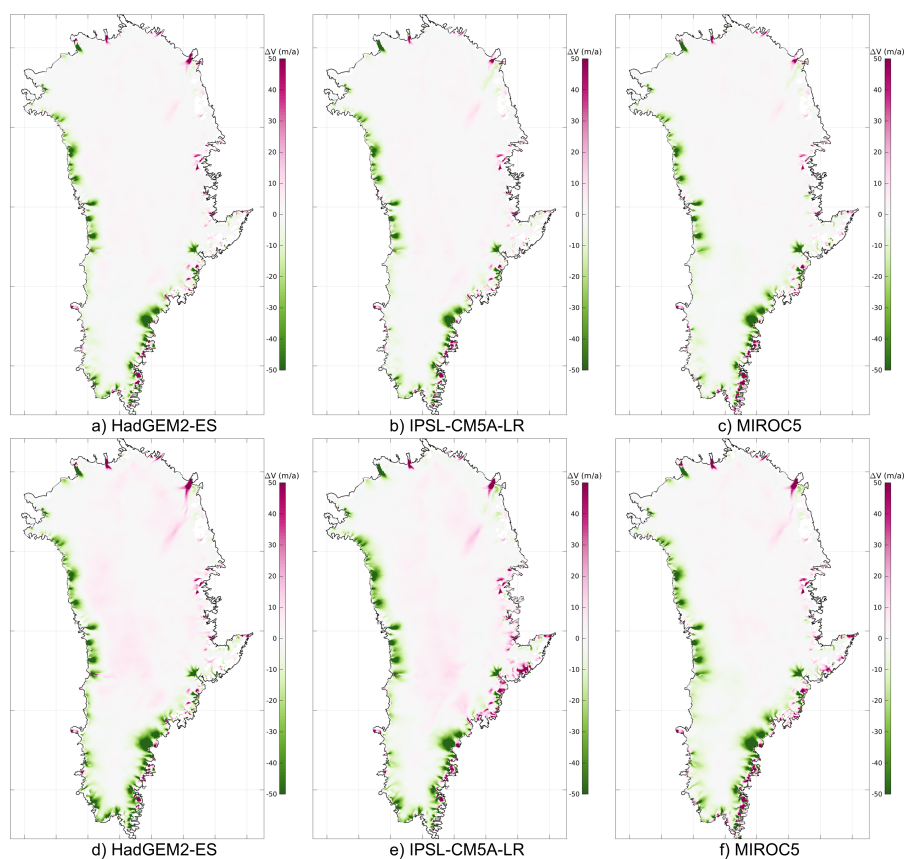


Figure 10. Comparison of multi-year mean surface velocity (v) differences between 2100-2000 (top row) and 2300-2000 (bottom row) for (a,d) HadGEM2-ES, (b,e) IPSL-CM5A-LR and (c,f) MIROC5. The black contour line depicts the present-day ice mask.